Biochemistry

 Volume 31, Number 23 June 16, 1992

Accelerated Publications

Secondary Structure and Topology of Interleukin-1 Receptor Antagonist Protein Determined by Heteronuclear Three-Dimensional NMR Spectroscopy

Brian J. Stockman,*,‡ Terrence A. Scahill,‡ Melinda Roy,§ Eldon L. Ulrich,§ Nancy A. Strakalaitis,∥ David P. Brunner,∥ Anthony W. Yem,‡ and Martin R. Deibel, Jr.‡

Upjohn Laboratories, Control Division, and Chemical Division, The Upjohn Company, 301 Henrietta Street, Kalamazoo, Michigan 49007

Received March 25, 1992; Revised Manuscript Received April 22, 1992

ABSTRACT: Interleukin-1 (IL-1) proteins, such as IL-1β, play a key role in immune and inflammatory responses. Interaction of these cytokines with the IL-1 receptor induces a variety of biological changes in neurologic, metabolic, hematologic, and endocrinologic systems. Interleukin-1 receptor antagonist protein (IRAP) is a naturally occurring inhibitor of the interleukin-1 receptor. The 153-residue protein binds to the receptor with an affinity similar to that of IL-1β but does not elicit any physiological responses. As a first step toward understanding IRAP's mode of action, we have used multidimensional, heteronuclear NMR spectroscopy to determine the antagonist's solution secondary structure and global fold. Using a combination of 3D ^{1}H–^{15}N NOESY–HMQC and TOCSY–HMQC and 3D ^{1}H–^{15}N–^{13}C HNCA and HN(CO)CA experiments on uniformly ^{15}N- or doubly $^{13}C/^{15}N$-enriched IRAP, we have made resonance assignments for more than 90% of the main-chain atoms. Analysis of short- and long-range NOE's indicates that IRAP is predominantly β-sheet, with the same overall topology as IL-1β but with different regions of the primary sequence comprising the β-strands. Two short helical segments also were identified. The 14% sequence identity between IL-1β and IRAP increases to 25% when differences in the locations of secondary structure elements in the primary sequences are taken into account. Still, numerous differences in side chains, which ultimately play a major role in receptor interaction, exist. Comparison of the structure of IRAP with that of IL-1β provides a basis for understanding the structure/function relationships at the molecular level that account for the drastically different physiological effects of these two proteins.

Interleukin-1α and interleukin-1β are two polypeptides which share a significant number of inflammatory, immunological, and pathological properties [for a review, see Dinarello (1989)]. Importantly, these dissimilar 17-kDa proteins bind to two classes of IL-1[1] receptors, resulting in the mediation of several immune and inflammatory responses and in the induction of a variety of biological changes in neurologic, metabolic, hematologic, and endocrinologic systems (Dinarello, 1989). In addition to IL-1α and IL-1β, an interleukin-1 receptor antagonist protein (termed either IRAP or IL-1ra) has been isolated, characterized, cloned, and expressed in *Escherichia coli* (Hannum et al., 1990; Eisenberg et al., 1990; Carter et al., 1990). This newer member of the IL-1 gene family is a naturally occurring inhibitor of the interleukin-1 receptor (Hannum et al., 1990; Carter et al., 1990) and represents the first described naturally occurring cytokine that

* To whom correspondence should be addressed.
‡ Upjohn Laboratories.
§ Control Division.
∥ Chemical Division.

[1] Abbreviations: DANTE, delays alternating with nutation for tailored excitation; DQF-COSY, double-quantum-filtered correlation spectroscopy; GARP, globally optimized alternating phase rectangular pulse; HMQC, heteronuclear multiple-quantum correlation; HNCA, three-dimensional NMR experiment correlating $^{1}H^{N}$ and $^{15}N^{\alpha}$ resonances of a given residue with the $^{13}C^{\alpha}$ resonances of the same and preceding residues; HN(CO)CA, three-dimensional NMR experiment correlating $^{1}H^{N}$ and $^{15}N^{\alpha}$ resonances of a given residue with the $^{13}C^{\alpha}$ resonance of the preceding residue; HSQC, heteronuclear single-quantum correlation; IL-1, interleukin-1; IL-1α, interleukin-1α; IL-1β, interleukin-1β; IRAP, interleukin-1 receptor antagonist protein; NMR, nuclear magnetic resonance; NOESY, nuclear Overhauser enhancement spectroscopy; NOE, nuclear Overhauser enhancement; SCUBA, stimulated cross peaks under bleached α's; TMS, tetramethylsilane; TOCSY, total correlation spectroscopy; TPPI, time-proportional phase incrementation; $d_{XY}(a,b)$, NOE between proton X on residue a and proton Y on residue b.

0006-2960/92/0431-5237$03.00/0

functions entirely as a specific receptor antagonist.

IRAP is synthesized and secreted from human monocytes and macrophages as a 17–25-kDa variably glycosylated protein (Arend, 1991), a distinction from that of both IL-1α and IL-1β. However, as discovered with the recombinant form of the protein, the carbohydrate moieties are not required for IL-1 antagonist activities. The mature IRAP protein is a 152 amino acid polypeptide with a leader sequence of 25 amino acids (Eisenberg et al., 1990), showing between 26% and 30% sequence homology to IL-1β and 19% to IL-1α (Eisenberg et al., 1990). The recombinant IRAP protein itself is a 153-residue polypeptide that binds with high affinity (comparable to that of IL-1α and IL-1β) to both types of IL-1 receptors.

Site-directed mutagenesis (MacDonald et al., 1986; Wingfield et al., 1989; Gehrke et al., 1990) and protein modification (Wingfield et al., 1989) studies have identified three regions of IL-1β that are involved in either receptor binding or transmission of the biological response upon binding. For IRAP, it can be hypothesized that the regions of structure important for receptor binding are maintained but that the region or regions responsible for eliciting the response are somehow different. To this end, we have begun an intensive program to determine the solution structure of IRAP using NMR spectroscopy. Since the solution (Driscoll et al., 1990a,b; Clore et al., 1991a,b; Tate et al., 1992) and crystalline (Finzel et al., 1989; Priestle et al., 1989) structures of IL-1β have been determined, direct comparisons can be made between IRAP and IL-1β. This may lead to a correlation between structural and biological differences.

Materials and Methods

Protein Enrichment and Sample Preparation. Expression of IRAP was carried out using *E. coli* K-12 strain DU379. This strain carries the vector pUC-ILinh and mediates heterologous expression via the *E. coli trp* promoter. Small-scale stirred-tank fermentations were conducted at the 1.5-L scale in a defined salts medium derived from NS85 medium and optimized for the highest level of expression while minimizing the possibility of isotopic dilution. The fermentation media were supplemented with $(^{15}NH_4)_2SO_4$, [$^{13}C_1$]- and/or [^{15}N]-L-methionine, $^{15}NH_4Cl$, and [^{13}C]-D-glucose (stable isotopes were obtained from Cambridge Isotope Laboratories, Isotec, and/or MSD Isotopes) as required to produce either ^{15}N- or doubly $^{13}C/^{15}N$-enriched IRAP. Analysis of resolved ^1H resonances indicated that both ^{13}C and ^{15}N were incorporated at an enrichment level greater than 95%. Fermentations were conducted by growth of the DU379 culture at 30 °C to a density of 5 A_{550}, followed by a temperature shift to 37 °C. The level of heterologous expression was further modulated by L-tryptophan control of the *E. coli trp* promoter. Since the media contained excess methionine and tryptophan present at natural abundance levels of ^{13}C (except at the carbonyl carbon of methionine), the $^{13}C^{\alpha}$ resonances of IRAP methionine and tryptophan residues were not detected in the triple-resonance experiments described below. Following ca. 25 h of incubation, the bacterial population was harvested by centrifuging, the bacterial paste was subjected to four cycles of freeze/thaw extraction, and IRAP was purified as described previously (Carter et al., 1990).

NMR samples were prepared by dialyzing 20 mg of purified IRAP four times against 250 mL of 100 mM NaCl. [$^2H_4$]-Ethanolamine stock solution at pH 6.4 was then added so that after the sample was concentrated under a stream of nitrogen gas the resulting solution (400 μL of ^1H_2O plus 40 μL of ^2H_2O for the deuterium lock signal used by the spectrometer) was 2 mM IRAP, 50 mM [$^2H_4$]ethanolamine, and 300 mM NaCl. Trace amounts of PMSF and NaN_3 were added to prevent any protease digestion or bacterial growth in the sample. Samples dissolved in 100% ^2H_2O were prepared over a time period of 5–6 h by repeated concentration of the solution under a stream of nitrogen gas and addition of ^2H_2O.

NMR Spectroscopy. All NMR spectra were recorded at 27 °C on a Bruker AMX-600 spectrometer equipped with a triple-resonance probe and a multichannel interface. Proton chemical shifts are referenced to the ^1H_2O signal at 4.76 ppm. Nitrogen chemical shifts are referenced to external $^{15}NH_4Cl$ (2.9 M) in 1 M HCl at 24.93 ppm relative to liquid ammonia. Carbon chemical shifts are referenced to 10% dioxane in ^2H_2O at 67.8 ppm relative to TMS. Data were processed using the software package FELIX from Hare Research, Inc.

Two-dimensional phase-sensitive ^1H–^1H DQF-COSY (Piantini et al., 1982) and NOESY (Anil Kumar et al., 1980) spectra were recorded using standard pulse sequences. Two dimensional heteronuclear ^1H–^{15}N HSQC spectra were recorded using single-quantum magnetization transfer (Bodenhausen & Ruben, 1980) in order to obtain favorable line widths (Bax et al., 1990). Continuous-wave low-power saturation was used during the 1.3-s relaxation delay to reduce the intensity of the ^1H_2O resonance. GARP decoupling (Shaka et al., 1985) was used during acquisition to decouple ^{15}N. ^1H–^{15}N HSQC spectra were recorded on IRAP in ^1H_2O and ^2H_2O in order to determine which $^1H^N$ resonances had reduced solvent-exchange rates.

Three-dimensional ^1H–^{15}N NOESY–HMQC and TOCSY–HMQC experiments were recorded with slight modification (Clubb et al., 1991) of the methods of Zuiderweg and Fesik (1989) and Marion et al. (1989). The SCUBA method (Brown et al., 1988) was used to recover intensity of saturated $^1H^{\alpha}$ resonances resulting from irradiation of the solvent line during the 1.3-s relaxation delay. Decoupling of ^{15}N during the t_1 period was accomplished with a 180° ^{15}N pulse in the center of this evolution period and during acquisition with a GARP sequence. Sweep widths of 7353, 1562, and 9090 Hz were used in the ω_1, ω_2, and ω_3 dimensions, respectively. Quadrature in t_1 and t_2 was obtained with TPPI (Marion & Wüthrich, 1983). Each 3D spectrum was collected as a series of 32 two-dimensional ^1H–^1H experiments, consisting of 32 scans (1024 complex data points) for each of 256 t_1 increments. The mixing time for the NOESY data set was 100 ms. The isotropic mixing time for the TOCSY data set was 33 ms and employed the DIPSI-2 (Shaka et al., 1988) mixing scheme. The duration of each three-dimensional experiment was 120 h.

Three-dimensional ^1H–^{15}N–^{13}C HNCA and HN(CO)CA triple-resonance experiments were recorded with constant-time ^{15}N evolution as described by Grzesiek and Bax (1992). Both the HNCA and HN(CO)CA experiments consisted of 64 ^{15}N t_1 values and 64 ^{13}C t_2 values, with 32 scans acquired for each (t_1, t_2) increment. Quadrature in t_1 and t_2 was obtained with TPPI. The 90° ^{13}C pulse width used was 55 μs. This results in pulses centered on the $^{13}C^{\alpha}$'s having a null at the carbonyl carbons and vice versa. In each experiment, the carbon carrier frequency was centered in the $^{13}C^{\alpha}$ region. Carbonyl pulses were achieved in a DANTE fashion (Morris & Freeman, 1978), with six 60°-phase-shifted pulses comprising each off-resonance 90° DANTE pulse. Low-power presaturation was used to reduce the intensity of the water resonance. WALTZ-16 (Shaka et al., 1983) decoupling was used during acquisition to decouple ^{15}N.

Results

Assignment of the majority of the backbone ^1H, ^{13}C, and

^{15}N resonances of IRAP was accomplished by analysis of four three-dimensional data sets. First, ^{1}H–^{15}N NOESY–HMQC and TOCSY–HMQC experiments were recorded on uniformly ^{15}N-enriched IRAP. Then, two ^{1}H–^{15}N–^{13}C triple-resonance experiments were recorded, the so-called HNCA and HN(CO)CA experiments (Ikura et al., 1990; Bax & Ikura, 1991). Redundant sequential connectivities obtained from the heteronuclear data sets simplified and increased the reliability of the assignments. During the assignment process, NOE's indicative of secondary structure were identified.

Analysis of the ^{1}H–^{15}N NOESY–HMQC and TOCSY–HMQC data sets consisted of five steps: (1) intraresidue and interresidue cross peaks to each amide proton in the NOESY–HMQC spectrum were distinguished by cross reference to the corresponding amide proton resonance in the TOCSY–HMQC spectrum, which contains only intraresidue correlations, (2) NOE's between NH protons, often indicative of sequentially or cross-β-strand adjacent amide protons, were identified, (3) sequential stretches of residues were aligned by analysis of interresidue NOE's (Wüthrich, 1986), (4) classification of several of the NH groups in each stretch as alanine, valine, or AMX, based on analysis of DQF-COSY and TOCSY data sets, was done, and (5) sequence-specific placement of the stretches based on the uniqueness of the primary sequence was determined. An example of this kind of analysis for residues 31–36 of IRAP is shown in Figure 1. Each panel represents a small ω_1, ω_3 slice of the ^{1}H–^{15}N NOESY–HMQC spectrum corresponding to the NH group of the residue indicated. Intraresidue NOE's are boxed. Arrows drawn indicate sequential NOE's used to make the assignments. Analysis of these two three-dimensional data sets resulted in backbone assignments for approximately 60% of the residues. Assignments for the remaining residues, some of which were aligned in stretches but not placed in the primary sequence, were ambiguous with these data alone.

To complete the main-chain assignments, two triple-resonance experiments (Grzesiek & Bax, 1992; Ikura et al., 1990) were recorded on uniformly $^{13}C/^{15}N$-enriched IRAP: HNCA, which correlates the $^{1}H^{N}$, $^{15}N^{\alpha}$, and $^{13}C^{\alpha}$-chemical shifts of a given residue and, in most cases, the $^{13}C^{\alpha}$ chemical shift of the preceding residue, and HN(CO)CA, which correlates the $^{1}H^{N}$ and $^{15}N^{\alpha}$ chemical shifts of a given residue with the $^{13}C^{\alpha}$ chemical shift of just the preceding residue. The HNCA and HN(CO)CA experiments were analyzed in parallel, in much the time same way as the NOESY–HMQC and TOCSY–HMQC data sets. For IRAP, each NH resonance gave rise to two $^{13}C^{\alpha}$ correlations in the HNCA spectrum (except for residues preceded by a methionine or tryptophan). The interresidue and intraresidue $^{13}C^{\alpha}$ correlations were distinguished by locating the same NH group in the HN(CO)CA spectrum, which gives correlations to only the interresidue $^{13}C^{\alpha}$. An example of this kind of analysis for residues 40–45 of IRAP is shown in Figure 2. Each panel in (A) represents a small ω_2, ω_3 slice of the HNCA spectrum corresponding to the NH group of the residue indicated. Boxes denote the interresidue $^{13}C^{\alpha}$ resonance, determined by reference to the corresponding panel from the HN(CO)CA spectrum in (B). In most cases, the intensity of the interresidue correlation is less than that of the intraresidue correlation. Careful analysis of the HNCA and HN(CO)CA data sets confirmed the assigments made with the ^{1}H–^{15}N data sets and extended the assigments to 90% of the residues. For all residues assigned, the $^{13}C^{\alpha}$ chemical shifts, which have been recently shown to have a secondary-structure-dependent range (Spera & Bax, 1991), were consistent with those expected. In fact, characteristic $^{13}C^{\alpha}$

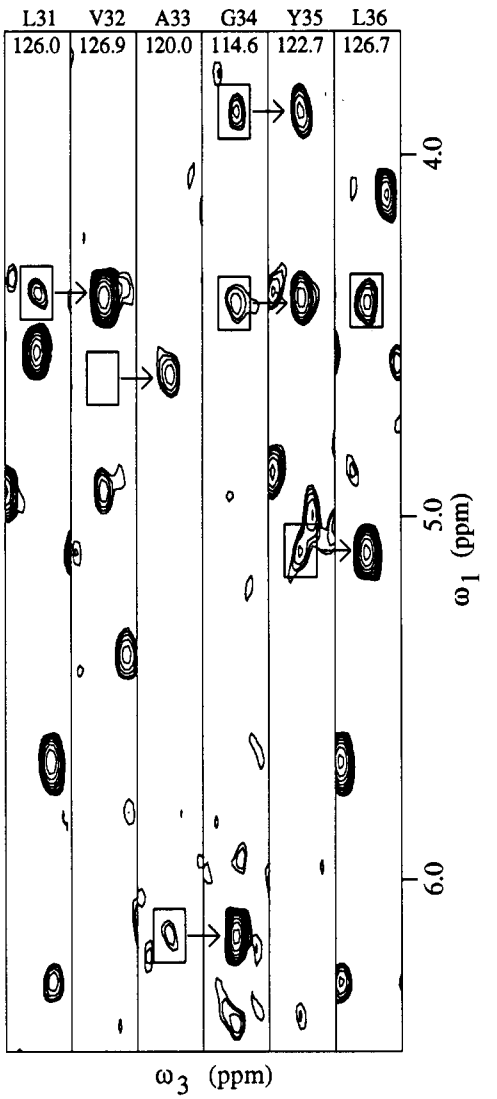

FIGURE 1: Selected ω_1, ω_3 slices taken from the 14.2-T three-dimensional ^{1}H–^{15}N NOESY–HMQC spectrum of IRAP. Slices are taken at the ω_2 (^{15}N) frequency shown and correspond to the residue indicated at the top. Each slice represents 0.24 ppm in ω_3, with the center located at the frequency of the indicated $^{1}H^{N}$ resonance (listed in Table I). Intraresidue $d_{N\alpha}$ correlations are boxed. Sequential interresidue $d_{N\alpha}(i,i-1)$ correlations are indicated by arrows beginning at the boxed intraresidue correlation in the preceding slice. In the V32 slice, the weak $d_{N\alpha}$ correlation is not seen at this level; an intense correlation is seen at the corresponding position in the ^{1}H–^{15}N TOCSY–HMQC spectrum.

chemical shifts aided the analysis by restricting the possibilities of the type of amino acid involved in many correlations. A summary of the observed sequential connectivities is presented in Figure 3.

For many residues, magnetization transfer in the ^{1}H–^{15}N TOCSY–HMQC spectrum extended resonance assignments to at least one $^{1}H^{\beta}$ resonance and sometimes even further down the side chain. In cases of favorable resolution, such as for high-field shifted resonances, two-dimensional DQF-COSY and TOCSY spectra confirmed and/or extended these side-chain assignments. Extensive side-chain assignments, however, will require ^{13}C-directed strategies (Fesik et al., 1990; Kay et al., 1990) and are currently in progress. Chemical shifts of assigned backbone and side-chain resonances are listed in Table I.

Once the majority of correlations were assigned in the ^{1}H–^{15}N HSQC spectrum recorded in $^{1}H_2O$, an identical spectrum was recorded after the protein was exchanged into $^{2}H_2O$. As

Table I: Chemical Shifts of Assigned ^{1}H, ^{13}C, and ^{15}N Resonances of IRAP[a]

residue	N^{α}	H^{N}	C^{α}	H^{α}	H^{β}	others
Met 11	120.8	8.00		4.90	1.82, 2.01	
Gln 12	125.8	9.21	53.1	4.68	2.10	
Ala 13	127.8	8.64	49.9	5.42	1.37	
Phe 14	124.9	9.75	55.0	4.76	1.99, 2.41	H^{δ} 6.26
Arg 15	120.4	9.08	52.9	5.22	1.76	
Ile 16	121.8	9.09	57.1	5.78		
Trp 17	125.3	8.65		5.48	3.06, 3.65	$H^{\delta 1}$ 7.34; $H^{\epsilon 2}$ 7.20; $H^{\eta 2}$ 7.03; $H^{\epsilon 3}$ 7.45; $H^{\zeta 3}$ 6.81; $H^{\epsilon 1}$ 9.68
Asp 18	121.6	9.41	51.3	5.08	2.72, 2.92	
Val 19	110.7	6.78	62.7	4.23	2.28	H^{γ} 0.75, 0.88
Asn 20	120.7	8.38	51.2	5.22	2.70, 3.26	
Gln 21	114.6	8.89	56.4	4.06	2.73	
Lys 22	120.9	8.69	56.2	4.12	2.08	
Thr 23	114.9	8.93	58.5	4.97	4.43	H^{γ} 1.32
Phe 24	123.6	9.60	51.9	5.97	2.96, 3.41	
Tyr 25	117.8	9.13	54.6	5.01	2.90, 3.14	
Leu 26	122.3	9.23	52.0	4.95	1.38, 1.74	
Arg 27	125.4	8.91	53.7	4.55	1.70	
Asn 28			53.1			
Asn 29	111.6	8.86	53.1	4.13	2.86, 3.04	
Gln 30	118.2	7.67	52.2	4.58	1.90, 2.30	
Leu 31	126.0	8.80	53.2	4.41	1.44	
Val 32	126.9	9.18	58.0	4.64	1.22	H^{γ} 0.02, 0.45
Ala 33	120.0	7.28	47.3	6.13	1.39	
Gly 34	114.6	9.85	43.8	3.92, 4.43		
Tyr 35	122.7	9.27	55.3	5.10	2.82, 3.15	
Leu 36	126.7	8.68	52.3	4.42	1.76	
Gln 37	121.3	8.46	52.5	4.59	1.95, 2.12	H^{γ} 2.28
Gly 38						
Pro 39			62.5			
Asn 40	115.8	7.72	52.1	4.70	2.99	
Val 41	117.3	7.46	63.5	3.82	2.21	H^{γ} 0.97
Asn 42	118.9	7.79	52.9	4.65	2.90	
Leu 43	120.1	7.86	53.3	4.36	1.86	
Glu 44	120.7	7.15	55.8	4.19		
Glu 45	128.9	8.88	53.1	4.90		
Lys 46	124.7	8.07	54.2	4.78		
Ile 47	123.0	9.15	55.7	5.01	2.01	$H^{\gamma 2}$ 0.95
Asp 48	130.3	9.28	52.4	5.19	2.00, 2.58	
Val 49	121.3	8.82	58.8	5.22	2.05	H^{γ} 0.90
Val 50	126.7	8.00	57.6	4.85	2.13	
Pro 51			61.1			
Ile 52	124.1	8.40	58.3	4.16	1.37	$H^{\gamma 2}$ 0.60
Glu 53	125.8	8.60	53.6	4.39		
Pro 54						
His 55			54.8			
Ala 56	123.5	8.28	48.9	5.64	1.22	
Leu 57	119.6	9.30	53.7	4.96	1.92	
Phe 58	121.2	8.60	54.7	5.56	2.72	
Leu 59	123.6	10.30	52.4	5.22		
Gly 60	111.4	9.28	44.0	3.99, 5.01		
Ile 61	111.6	8.86	58.4	5.34		
His 62	116.9	9.75	53.9	4.56		
Gly 63	112.8	9.23	44.9	3.80, 3.93		
Gly 64	109.6	8.36	43.8	3.25, 4.15		
Lys 65	117.5	7.30	55.3	4.39	1.85	
Met 66	117.6	7.65		5.35		
Cys 67	118.9	9.08	56.9	5.50	2.41, 2.83	
Leu 68	126.0	8.50	54.4	4.96		
Ser 69	113.5	9.06	54.0	5.15		
Cys 70	117.6	7.47	52.2	4.88	2.79, 3.11	
Val 71	127.5	8.72	59.0	4.10	1.65	H^{γ} 0.65
Lys 72	127.0	8.21	52.9	4.82	1.54, 1.66	
Ser 73	120.8	8.26	54.7	4.52	3.61	
Gly 74						
Asp 75			52.9			
Glu 76	121.7	8.05	54.2	4.49	2.03	
Thr 77	122.5	7.97	60.9	4.12	2.29	H^{γ} −0.2
Arg 78	124.8	8.56	52.6	4.63	1.61	
Leu 79	124.5	8.62	51.7	5.05	1.85	
Gln 80	128.4	9.08	52.4	4.66	1.90, 2.08	
Leu 81	124.3	8.28	51.9	4.95		
Glu 82	124.5	9.17	53.7	4.76	2.05, 2.23	
Ala 83	129.8	8.95	50.1	4.88	1.38	
Val 84	126.5	7.72	58.2	4.12	1.76	H^{γ} 0.55
Asn 85	121.7	8.22	50.3	5.02	2.60, 2.70	
Ile 86	129.5	9.01	62.9	3.67		
Thr 87	110.0	7.46	61.5	4.13	4.42	H^{γ} 1.21

Table I (Continued)

residue	N^{α}	H^{N}	C^{α}	H^{α}	H^{β}	others
Asp 88	122.0	7.93	52.8	4.74	2.70	
Leu 89	121.6	6.50	52.6	4.10	0.85	
Ser 90	118.5	10.08	54.7	4.99	3.62	
Glu 91	129.5	10.01	56.5	4.24	2.01, 2.21	
Asn 92	117.6	8.22	51.6	4.84	2.59, 2.95	
Arg 93	122.4	7.41	53.9	4.65	1.79, 2.07	
Lys 94						
Gln 95			57.1			
Asp 96	121.0	7.65	53.5	4.96	2.90, 3.39	
Lys 97	123.2	7.68	57.5	4.00		
Arg 98	114.1	7.49	56.3	4.06		
Phe 99	122.5	7.86	56.7	5.32	3.05	
Ala 100	122.5	7.96	50.3	4.99	1.22	
Phe 101	124.8	9.66	55.2	5.18	2.80	
Ile 102	123.0	10.18	59.3	4.34	1.83	$H^{\gamma 2}$ 0.91
Arg 103	131.8	9.06	53.8	4.76	1.78	
Ser 104	122.9	8.59	55.4	4.70	3.76	
Asp 105	125.3	8.67	52.0	5.46	2.46, 2.75	
Ser 106	118.6	8.51	54.6	4.58	3.59	
Gly 107						
Pro 108			62.1			
Thr 109	110.4	7.58	58.3	4.79	3.90	H^{γ} 0.41
Thr 110	120.8	9.72	60.7	5.07	3.28	H^{γ} 0.47
Ser 111	121.6	8.79	55.6	5.14	3.76	
Phe 112	120.6	9.76	54.7	5.38	2.76	
Glu 113	127.6	9.11	51.8	4.37	1.63	
Ser 114	122.3	8.90	56.9	3.64		
Ala 115	129.9	8.23	52.0	4.05	1.21	
Ala 116	117.4	7.12	50.9	4.13	1.27	
Cys 117	119.5	7.84	48.1	4.51	2.90	
Pro 118			62.5			
Gly 119	114.2	10.22	42.8	3.45, 4.19		
Trp 120	121.3	8.15		4.77	2.86, 3.58	$H^{\delta 1}$ 6.97; $H^{\zeta 2}$ 7.51; $H^{\eta 2}$ 7.23; $H^{\epsilon 3}$ 7.08; $H^{\epsilon 1}$ 10.05
Phe 121	123.0	9.50	54.7	5.59	2.76	
Leu 122	126.4	8.95	54.4	4.76		
Cys 123	121.6	9.08	54.1	6.30	2.79, 3.00	
Thr 124	110.7	9.15	56.5	4.90	4.40	H^{γ} 1.39
Ala 125	123.7	9.38	48.7	4.85	1.59	
Met 126	118.9	8.70		4.16	2.09	
Glu 127	120.4	7.95	54.7	4.38	2.03	
Ala 128	125.0	8.88	51.5	3.97	1.72	
Asp 129	116.1	8.68	54.8	4.02	2.83, 2.99	
Gln 130	118.1	8.64	50.4	4.78	1.87	
Pro 131			61.6			
Val 132	129.0	8.13	62.7	3.95	1.21	H^{γ} −0.06, 0.68
Ser 133	124.8	9.05	54.6	4.85	3.64	
Leu 134	118.6	8.51	51.9	5.81	1.78	
Thr 135	116.2	9.47	58.6	5.18	4.41	H^{γ} 0.96
Asn 136	128.7	7.37	49.2	5.22		
Met 137	120.7	8.30		4.97	1.80	
Pro 138			63.0			
Asp 139	119.0	8.48	53.2	4.65	2.53, 2.75	
Glu 140	120.0	7.58	55.3	4.29	1.97, 2.13	
Gly 141	108.3	8.13	44.0	3.96, 4.07		
Val 142	117.6	7.80	61.6	4.21	2.22	H^{γ} 0.95
Met 143	118.5	7.98		5.05	1.83, 2.08	H^{γ} 2.78
Val 144	126.6	9.65	61.2	4.08	2.71	H^{γ} 0.69, 0.76
Thr 145	113.3	8.42	58.7	5.09		
Lys 146	124.4	6.72	54.0	4.52	1.50	
Phe 147	119.0	8.88	54.7	4.83	2.53	
Tyr 148	123.0	9.50	56.6	4.50		
Phe 149	128.6	8.76	54.0	5.68	3.22	
Gln 150	126.4	8.76	52.6	4.79	1.98, 2.15	H^{γ} 2.39
Glu 151	130.1	9.20	56.3	2.95		
Asp 152	127.3	8.56	52.3	4.60	2.50	
Glu 153	128.6	7.78	56.2	4.10	1.83, 1.99	H^{γ} 2.15

[a] Proton chemical shifts are ±0.02 ppm. Carbon and nitrogen chemical shifts are ±0.1 ppm. Residues 1–10 have not been assigned.

described under Materials and Methods, this process took 6 h to complete, so that by the time the first ^{1}H–^{15}N HSQC spectrum could be recorded, all of the fast-exchanging NH protons had been replaced by deuterons and were not observed in the spectrum. Only 50 ^{1}H–^{15}N correlations remained after this amount of time in $^{2}H_2O$ solvent. Residues with slowly-exchanging NH protons are indicated with filled circles in Figure 3. As discussed below, each of these residues was found to participate in the β-sheet framework of IRAP.

Remaining unassigned residues are clustered in three locations: 1–10, 74–75, and 94–95. The N-terminus is by far the longest stretch that has so far resisted assignment. Several unassigned correlations remain in the ^{1}H–^{15}N HSQC spectrum, although they are of weaker intensity than those already

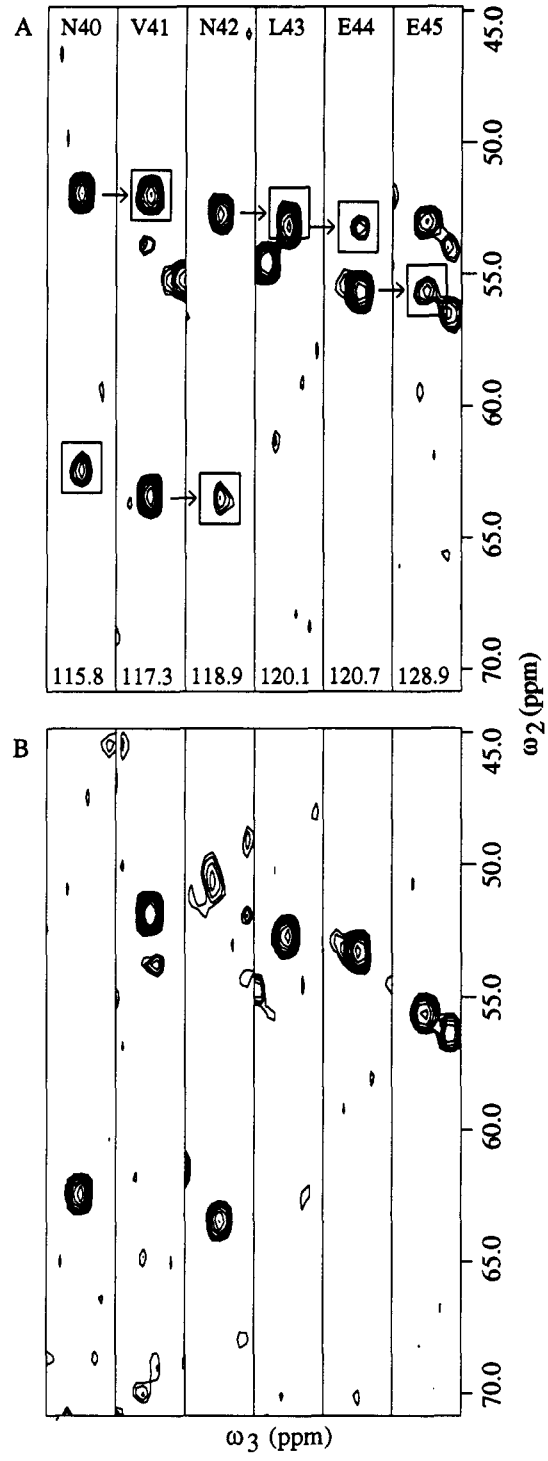

FIGURE 2: Selected ω_2, ω_3 slices taken from the 14.2-T three-dimensional ^1H–^{15}N–^{13}C HNCA (A) and HN(CO)CA (B) spectra of IRAP. Slices are taken at the ω_1 (^{15}N) frequency indicated at the bottom of (A) and correspond to the residue indicated at the top of (A). Each slice represents 0.32 ppm in ω_3, with the center located at the frequency of the indicated $^1H^N$ resonance (listed in Table I). Interresidue $H^N(i)C^\alpha(i-1)$ correlations in the HNCA spectrum are boxed. Arrows in the HNCA spectrum originate at the intraresidue H^NC^α correlation in a given slice and terminate at the interresidue $H^N(i)C^\alpha(i-1)$ correlation in the following slice.

assigned. Saturation transfer during the presaturation period may be occurring. Alternatively, heterogeneity of the N-terminal signals may exist. This could be caused by cis/trans isomerization involving proline-3, by residual proteases which are known to clip off the first seven residues, or by both. Evidence of cis/trans isomerization has also been observed in several assigned resonances and is currently being investigated in more detail.

Discussion

During analysis of the ^1H–^{15}N NOESY–HMQC data set, NOE's indicative of the solution secondary structure (Wüthrich, 1986) of IRAP were identified. The majority of these were classified as cross-strand NOE's between residues involved in β-sheet structure. They are manifested in the NOESY–HMQC spectrum as a third $^1H^\alpha$ NOE to an amide proton (the others being the interresidue and intraresidue $^1H^\alpha$'s) or as weak, nonsequential $^1H^N$–$^1H^N$ NOE's. Stretches of residues giving rise to these types of NOE's also had other characteristics associated with β-sheet residues: low-field $^1H^\alpha$ and $^1H^N$ chemical shifts, strong $^1H^N$–$^1H^\alpha$ coupling (manifested by intense DQF-COSY and TOCSY correlations), and reduced NH-exchange rates (see Figure 3). In addition, 22 intense $^1H^\alpha$–$^1H^\alpha$ NOE's, characteristic of antiparallel β-sheet (Wüthrich, 1986), were identified in the two-dimensional NOESY spectrum recorded in ^2H_2O. Analysis of this pattern of NOE's results in alignment of the 12 β-sheet strands as shown in Figure 4. Arrows indicate observed cross-strand NOE's, while dashed lines indicate hydrogen bonds inferred from NH-exchange rates. Overall, residues involved in the β-sheet framework had upfield-shifted $^{13}C^\alpha$ resonances (indicated by minus signs in Figure 3) compared to random coil values (Richarz & Wüthrich, 1978), as expected (Spera & Bax, 1991).

The β-sheet strands have been presented in Figure 4 in a manner that allows easy comparison to the β-sheet framework elucidated for IL-1β in solution by Driscoll et al. (1990b, Figure 5). Comparison of the two figures illustrates how the overall topology of the two proteins is identical, but in several regions is composed of different stretches of the primary sequence. Strands II and III, which are adjacent strands connected by a five-residue turn in IL-1β, are shifted by six residues in the primary sequence and are connected by a four-residue turn in IRAP. Similarly, strands I and IV in IRAP are shifted by six and five residues, respectively. The consequence of shifting the residues that comprise these portions of the β-sheet is that the N-terminal six residues of IRAP have no structural counterpart in the IL-1β structure. Structurally significant shifts of one residue are seen for strands VI, VII, and XII.

While the solution secondary structure of IRAP is dominated by antiparallel β-sheet, short stretches of strong $^1H^N$–$^1H^N$ NOE's between adjacent residues, indicative of a helical conformation, were also observed. As shown in Figure 3, these regions involve residues 40–45 and 86–89. In addition, NOE's from $^1H^N$ of L89 to $^1H^\alpha$ of I86 and from $^1H^N$ of E44 to $^1H^\alpha$ of V41, both medium-range NOE's characteristic of a helical conformation (Wüthrich, 1986), were observed. These were the only NOE's of this type unambiguously assigned. In addition, the $^{13}C^\alpha$ chemical shifts in these two stretches are shifted downfield slightly (indicated by plus signs in Figure 3) compared to their random coil values, as would be expected for a helical conformation (Spera & Bax, 1991). These residues correspond to residues 35–40 and 87–90 in IL-1β, the former of which is a 3_{10} helix in solution (Driscoll et al., 1990b). Isolated strong $^1H^N$–$^1H^N$ NOE's between two or three residues were also observed (Figure 3), and turn conformations were located at positions 18–22, 27–30, 62–65, and 116–118.

Mutations have defined three distinct regions of IL-1β and IRAP that are involved in either receptor binding or response elicitation (Clore et al., 1991; Labriola-Tompkins et al., 1991).

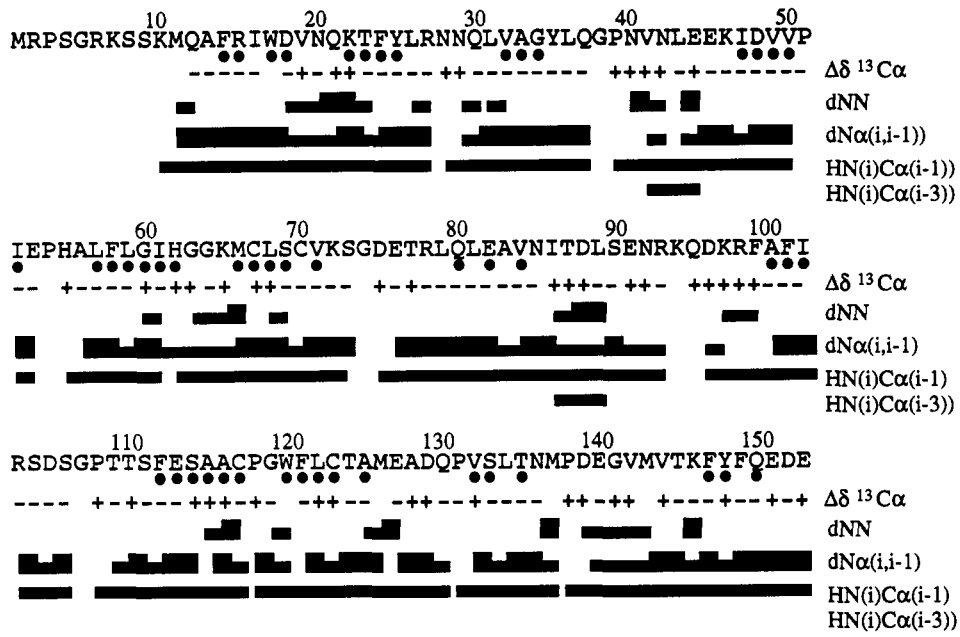

FIGURE 3: Summary of sequential resonance assignments of IRAP. A bar between two residues indicates that a d_{NN}, $d_{N\alpha}(i,i-1)$, or $d_{N\alpha}(i,i-3)$ NOE or $H^N(i)C^\alpha(i-1)$ correlation was observed between the two residues. For the d_{NN} and $d_{N\alpha}(i,i-1)$ NOE's, wide bars indicate a strong intensity NOE, while narrow bars indicate a weak or medium intensity NOE. Filled circles indicate residues with slowly exchanging amide protons. For each assigned residue, the sign of the secondary $^{13}C^\alpha$ chemical shift ($\Delta\delta$), defined as the difference between the observed and random coil chemical shift, is indicated.

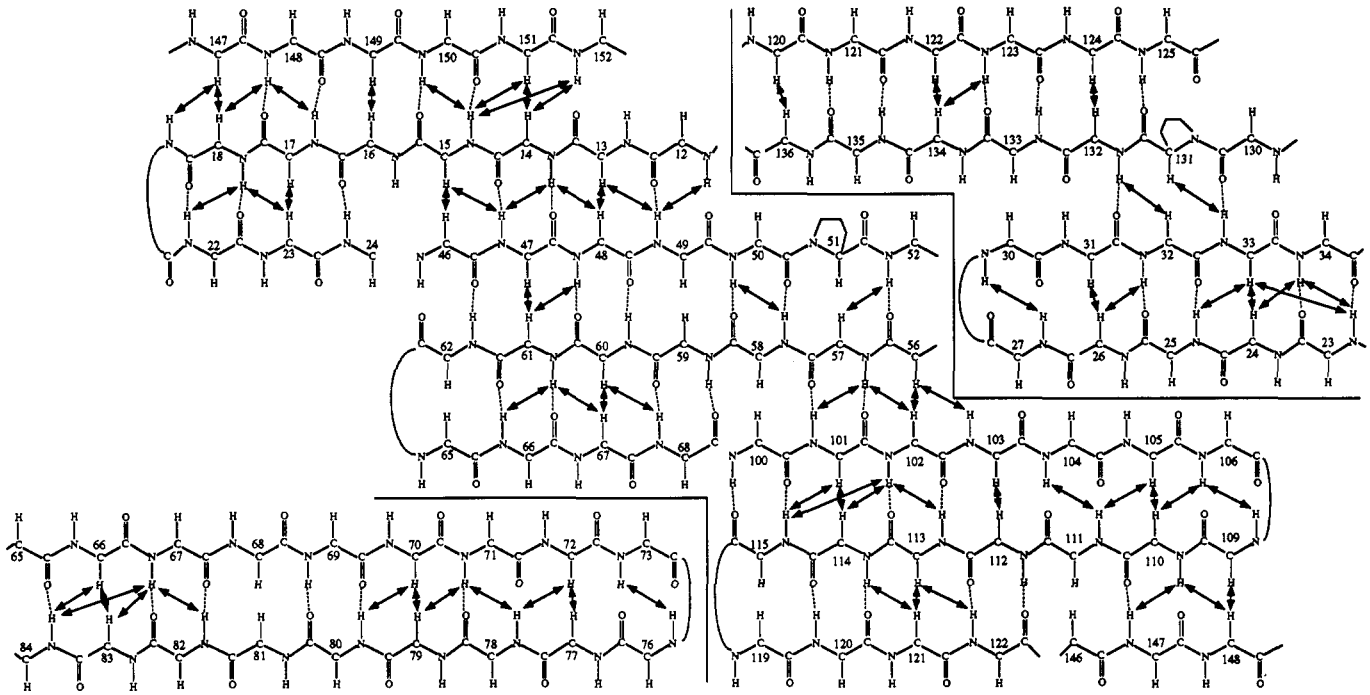

FIGURE 4: Schematic diagram of the topology of the β-sheet framework of IRAP. Residues comprising each strand are as follows: I, 12–18; II, 22–27; III 30–34; IV, 46–52; V, 56–62; VI, 65–73; VII, 76–84; VIII, 100–106; IX, 109–115; X, 119–125; XI, 130–136; XII, 146–152. Double-arrowhead lines identify assigned interstrand NOE's. Dashed lines indicate interstrand hydrogen bonds inferred from analysis of $^1H^N$ exchange rates (see Figure 3).

However, since the structure of only one of the two proteins was known, the relevance of the mutations to the very different physiological properties of the two proteins could not be determined. Comparison of the solution topology of IRAP presented here with that of IL-1β provides a basis to interpret the consequences of these mutations.

Site-directed mutagenesis has been used to define a discontinuous binding site on IL-1β for the type I IL-1 receptor (Labriola-Tompkins et al., 1991). It was found that amino acid substitutions involving R4, L6, F46, I56, K93, K103, and E105 drastically reduced IL-1β's binding ability. The structurally homologous residues in IRAP are K10, Q12, P51, H55, R93, R103, and D105, respectively. These residues are located on one face of IL-1β or IRAP. All four charged residues in IL-1β that were shown to be necessary for binding are structurally conserved in IRAP. This suggests that positively charged side chains at these positions are essential for receptor binding. Thus, the structural conservation of these residues may underlie IRAP's ability to mimic IL-1β and tightly bind the receptor.

In a separate study (Tate et al., 1992), a des-R98 mutant of IL-1β was shown to decrease IL-1β's binding ability. The structurally homologous residue in IRAP is also R98. NMR spectroscopy was used to show that truncation of up to seven N-terminal residues (including R4 and L6 discussed above) resulted in structural alterations that were localized to residues 41–47 and 86–99. This suggests that the overall structures of the truncation mutants are identical to wild-type IL-1β and that the observed reduction in binding results from deletion of key receptor-binding side chains and not a gross conformational change in the protein's structure. These results further emphasize the importance of positively-charged side chains in this region of the two cytokines as mediators of receptor binding.

Two other regions have been defined by mutagenesis to play a role in response elicitation, while not having a very large impact on receptor binding. Mutation of R11 to G11 and H30 to N30 or R30 in IL-1β reduces biological activity with only minimal effect on binding (MacDonald et al., 1986; Gehrke et al., 1990). The structurally analogous residues in IRAP are W17 (corresponding to R11) and Y35 (corresponding to H30). Lack of a charged side chain at residue 17 in IRAP may account for some loss of biological activity. A third region, however, seems to be the most critical with respect to biological activity. This region is defined by mutagenesis in IRAP of K146 to D146 (Ju et al., 1991). This mutation results in conversion of IRAP from an antagonist to a weak agonist of IL-1 for its receptor. Structurally, K146 in IRAP corresponds to D145 in IL-1β. The effect of the mutation is to change IRAP into IL-1β at this position, assuming that the mutated protein folds in the same conformation as wild-type IRAP. Thus the loss of biological activity in IRAP may be due in large part to the presence of a positively-charged side chain at residue 146.

The solution structure of IRAP presented here provides for a direct comparison with that of IL-1β. In the context of site-directed mutagenesis studies, structural differences and similarities between these two proteins that underlie their disparate functions can be analyzed in further detail.

Acknowledgments

We thank Dr. Paul E. Fagerness for NMR instrumentation support, Kathleen A. Farley for assistance with data analysis, Ron L. VanZanten for fermentation support, and Cindy A. Granatir for providing coordinates of an IRAP model based on the IL-1β structure. We also thank Dr. Ad Bax (NIH) for advice and for supplying preprints of the constant-time HNCA and HN(CO)CA pulse sequences.

References

Anil Kumar, Ernst, R. R., & Wüthrich, K. (1980) *Biochem. Biophys. Res. Commun. 95*, 1–6.

Arend, W. P. (1991) *J. Clin. Invest. 88*, 1445–1451.

Bax, A., & Ikura, M. (1991) *J. Biomol. NMR 1*, 99–104.

Bax, A., Ikura, M., Kay, L. E., Torchia, D. A., & Tschudin, R. (1990) *J. Magn. Reson. 86*, 304–318.

Bodenhausen, G., & Ruben, D. L. (1980) *Chem. Phys. Lett. 69*, 185–188.

Brown, S. C., Weber, P. L., & Mueller, L. (1988) *J. Magn. Reson. 77*, 166–169.

Carter, D. B., Deibel, M. R., Jr., Dunn, C. J., Tomich, C.-S. C., Laborde, A. L., Slightom, J. L., Berger, A. E., Bienkowski, M. J., Sun, F. F., McEwan, R. N., Harris, P. K. W., Yem, A. Y., Waszak, G. A., Chosay, J. G., Sieu, L. C., Hardee, M. M., Zurcher-Neely, H. A., Reardon, I. M., Heinrikson, R. L., Truesdell, S. E., Shelly, J A., Eessalu, T. E., Taylor, B. M., & Tracey, D. E. (1990) *Nature 344*, 633–638.

Clore, G. M., & Gronenborn, A. M. (1991) *J. Mol. Biol. 221*, 47–53.

Clore, G. M., Wingfield, P. T., & Gronenborn, A. M. (1991) *Biochemistry 30*, 2315–2323.

Clubb, R. T., Thanabal, V., Osborne, C., & Wagner, G. (1991) *Biochemistry 30*, 7718–7730.

Dinarello, C. A. (1989) *Adv. Immunol. 44*, 153–205.

Driscoll, P. C., Clore, G. M., Marion, D., Wingfield, P. T., & Gronenborn, A. M. (1990a) *Biochemistry 29*, 3542–3556.

Driscoll, P. C., Gronenborn, A. M., Wingfield, P. T., & Clore, G. M. (1990b) *Biochemistry 29*, 4668–4682.

Eisenberg, S. P., Evans, R. J., Arend, W. P., Verderber, E., Brewer, M. T., Hannum, C. H., & Thompson, R. C. (1990) *Nature 343*, 341–346.

Fesik, S. W., Eaton, H. L., Olejinczak, E. T., Zuiderweg, E. R. P., McIntosh, L. P., & Dahlquist, F. W. (1990) *J. Am. Chem. Soc. 112*, 886–888.

Finzel, B. C., Clancy, L. L., Holland, D. R., Muchmore, S. W., Watenpaugh, K. D., & Einspahr, H. M. (1989) *J. Mol. Biol. 209*, 779–791.

Gehrke, L., Jobling, S. A., Paik, L. S. K., McDonald, B., Rosenwasser, L. J., & Auron, P. E. (1990) *J. Biol. Chem. 265*, 5922–5925.

Grzesiek, S., & Bax, A. (1992) *J. Magn. Reson. 96*, 432–440.

Hannum, C. H., Wilcox, C. J., Arend, W. P., Joslin, F. G., Dripps, D. J., Heimdal, P. L., Armes, L. G., Sommer, A., Eisenberg, S. P., & Thompson, R. C (1990) *Nature 343*, 336–340.

Ikura, M., Kay, L. E., & Bax, A. (1990) *Biochemistry 29*, 4659–4667.

Ju, G., Labriola-Tompkins, E., Campen, C. A., Banjamin, W. R., Karas, J., Plocinski, J., Biondi, D., Kaffka, K. L., Kilian, P. L., Eisenberg, S. P., & Evans, R. J. (1991) *Proc. Natl. Acad. Sci. U.S.A. 88*, 2658–2662.

Kay, L. E., Ikura, M., & Bax, A. (1990) *J. Am. Chem. Soc. 112*, 888–889.

Labriola-Tompkins, E., Chandran, C., Kaffka, K. L., Biondi, D., Graves, B. J., Hatada, M., Madison, V. S., Karas, J., Kilian, P. L., & Ju, G. (1991) *Proc. Natl. Acad. Sci. U.S.A. 88*, 11182–11186.

MacDonald, H. R., Wingfield, P., Schmeissner, U., Shaw, A., Clore, G. M., & Gronenborn, A. M (1986) *FEBS Lett. 209*, 295–298.

Marion, D., & Wüthrich, K. (1983) *Biochem. Biophys. Res. Commun. 113*, 967–974.

Marion, D., Driscoll, P. E., Kay, L. E., Wingfield, P. T., Bax, A., Gronenborn, A. M., & Clore, G. M. (1989) *Biochemistry 28*, 6150–6156.

Morris, G.A., & Freeman, R. (1978) *J. Magn. Reson. 29*, 433–462.

Piantini, U., Sørensen, O. W., & Ernst, R. R. (1982) *J. Am. Chem. Soc. 104*, 6800–6801.

Priestle, J. P., Schär, H. P., & Grütter, M. G. (1989) *Proc. Natl. Acad. Sci. U.S.A. 86*, 9667–9671.

Richarz, R., & Wüthrich, K. (1978) *Biopolymers 17*, 2133–2141.

Shaka, A. J., Keeler, J., Frenkiel, T., & Freeman, R. (1983) *J. Magn. Reson. 52*, 335–338.

Shaka, A. J., Barker, P. B., & Freeman, R. (1985) *J. Magn. Reson. 64*, 547–552.

Shaka, A. J., Lee, C. J., & Pines, A. (1988) *J. Magn. Reson. 77*, 274–293.

Spera, S., & Bax, A. (1991) *J. Am. Chem. Soc. 113*, 5490–5492.
Tate, S., Kikumoto, Y., Ichikawa, S., Kaneko, M., Masui, Y., Kamogashira, T., Ouchi, M., Takahashi, S., & Inagaki, F. (1992) *Biochemistry 31*, 2435–2442.
Wingfield, P, Graber, P., Shaw, A. R., Gronenborn, A. M., Clore, G. M., & MacDonald, H. R. (1989) *Eur. J. Biochem. 179*, 565–571.
Wüthrich, K. (1986) *NMR of Proteins and Nucleic Acids*, Wiley, New York.
Zuiderweg, E. R. P., & Fesik, S. W. (1989) *Biochemistry 28*, 2387–2391.

Influence of Benzo[*a*]pyrene Diol Epoxide Chirality on Solution Conformations of DNA Covalent Adducts: The (−)-*trans-anti*-[BP]G·C Adduct Structure and Comparison with the (+)-*trans-anti*-[BP]G·C Enantiomer†

Carlos de los Santos,‡ Monique Cosman,‡ Brian E. Hingerty,§ Victor Ibanez,∥ Leonid A. Margulis,∥ Nicholas E. Geacintov,∥ Suse Broyde,⊥ and Dinshaw J. Patel*,‡

Department of Biochemistry and Molecular Biophysics, College of Physicians and Surgeons, Columbia University, New York, New York 10032, Health and Safety Research Division, Oak Ridge National Laboratory, Oak Ridge, Tennessee 37831, and Chemistry and Biology Department, New York University, New York, New York 10003

Received February 28, 1992; Revised Manuscript Received April 16, 1992

ABSTRACT: Benzo[*a*]pyrene (BP) is an environmental genotoxin, which, following metabolic activation to 7,8-diol 9,10-epoxide (BPDE) derivatives, forms covalent adducts with cellular DNA. A major fraction of adducts are derived from the binding of N^2 of guanine to the C^{10} position of BPDE. The mutagenic and carcinogenic potentials of these adducts are strongly dependent on the chirality at the four asymmetric benzylic carbon atoms. We report below on the combined NMR–energy minimization refinement characterization of the solution conformation of (−)-*trans-anti*-[BP]G positioned opposite C and flanked by G·C base pairs in the d(C1-C2-A3-T4-C5-[BP]G6-C7-T8-A9-C10-C11)·d(G12-G13-T14-A15-G16-C17-G18-A19-T20-G21-G22) duplex. Two-dimensional NMR techniques were applied to assign the exchangeable and non-exchangeable protons of the benzo[*a*]pyrenyl moiety and the nucleic acid in the modified duplex. These results establish Watson–Crick base pair alignment at the [BP]G6·C17 modification site, as well as the flanking C5·G18 and C7·G16 pairs within a regular right-handed helix. The solution structure of the (−)-*trans-anti*-[BP]G·C 11-mer duplex has been determined by incorporating intramolecular and intermolecular proton–proton distances defined by lower and upper bounds deduced from NOE buildup curves as constraints in energy minimization computations. The BP ring spans both strands of the duplex in the minor groove and is directed toward the 3′-end of the modified strand in the refined structure. One face of the BP ring of [BP]G6 stacks over the C17 residue across from it on the partner strand while the other face is exposed to solvent. The long axis of the BP ring makes an angle of approximately 40° with the average direction of the DNA helix axis and is readily accommodated within a widened minor groove of a minimally perturbed B-DNA helix. The present results on the (−)-*trans-anti*-BP-N^2-G adduct opposite C in which the BP ring is oriented toward the 3′-end of the modified strand contrast strikingly with our previous demonstration that the mirror image (+)-trans-anti stereoisomer within the same sequence context orients the BP ring toward the 5′-end of the modified strand [Cosman et al. (1992) *Proc. Natl. Acad. Sci. U.S.A. 89*, 1914–1918]. These orientational differences are due to the chiral characteristics of the two BPDE enantiomers and may have profound influences on the interaction of cellular enzyme systems with these two structurally different alignments of this bulky DNA lesion.

Chiral effects are critically important in many biological systems and interactions and are often the key factors in determining biological activity–structure relationships. Well-known examples include the metabolic stereoselective synthesis of oxygenated polycyclic aromatic derivatives (Conney, 1982; Singer & Grunberger, 1983), chiral recognition in xenobiotic metabolism and drug–receptor interactions (Testa, 1989), ligand–DNA interactions (Barton, 1989), the pharmacology of drug molecules (Campbell & Wilson, 1991), and the genotoxic, mutagenic, and tumorigenic properties of a variety of metabolites of aromatic compounds (Conney, 1982; Seiler, 1990).

A specific and extensively studied case is the stereoselective metabolism of the well-known environmental pollutant benzo[*a*]pyrene (BP) to four different benzo[*a*]pyrene-7,8-diol 9,10-epoxide stereoisomers, each of which is characterized by different mutagenic and tumorigenic activities (Conney, 1982) (Chart I). Particularly striking are the differences in the biological activities of the (+)- and (−)-enantiomers of the anti diastereomer 7β,8α-dihydroxy-9α,10α-epoxy-7,8,9,10-tetrahydrobenzo[*a*]pyrene [designated (+)-BPDE and (−)-BPDE], respectively. The (+)-BPDE enantiomer is highly tumorigenic

† This research was supported by NIH Grant CA-2111 and Columbia University Start-up Funds to D.J.P., by NIH Training Grant CA-09503 to M.C., by NIH Grant CA-20851 and DOE DE-FG02-88ER60405 Contract to N.E.G., by NIH Grant CA-28038, DOE DE-FG02-90ER60931 Contract, and NSF Grant DMB-8416009 to S.B., and by DOE DE-AC05-840R21400 Contract with Martin-Marietta Energy Systems to B.E.H.

‡ Columbia University.
§ Oak Ridge National Laboratory.
∥ Chemistry Department, New York University.
⊥ Biology Department, New York University.

0006-2960/92/0431-5245$03.00/0